ORNL/TM-2023/2851

Summary of Methodology for Mitigating Risks Associated with Licensing and Qualifying AM Nuclear Materials

Holden C. Hyer
Daniel C. Sweeney
Christian M. Petrie

March 2023

M3CR-22OR0403032

Approved for public release.
Distribution is unlimited.

OAK RIDGE National Laboratory

ORNL IS MANAGED BY UT-BATTELLE LLC FOR THE US DEPARTMENT OF ENERGY

DOCUMENT AVAILABILITY

Reports produced after January 1, 1996, are generally available free via OSTI.GOV.

Website www.osti.gov

Reports produced before January 1, 1996, may be purchased by members of the public from the following source:

National Technical Information Service
5285 Port Royal Road
Springfield, VA 22161
Telephone 703-605-6000 (1-800-553-6847)
TDD 703-487-4639
Fax 703-605-6900
E-mail info@ntis.gov
Website http://classic.ntis.gov/

Reports are available to US Department of Energy (DOE) employees, DOE contractors, Energy Technology Data Exchange representatives, and International Nuclear Information System representatives from the following source:

Office of Scientific and Technical Information
PO Box 62
Oak Ridge, TN 37831
Telephone 865-576-8401
Fax 865-576-5728
E-mail reports@osti.gov
Website https://www.osti.gov/

ORNL/TM-2023/2851

Advanced Materials and Manufacturing Technologies

SUMMARY OF METHODOLOGY FOR MITIGATING RISKS ASSOCIATED WITH LICENSING AND QUALIFYING AM NUCLEAR MATERIALS

Holden C. Hyer
Daniel C. Sweeney
Christian M. Petrie

March 2023

Milestone #: M3CR-22OR0403032

Prepared by
OAK RIDGE NATIONAL LABORATORY
Oak Ridge, TN 37831
managed by
UT-BATTELLE LLC
for the
US DEPARTMENT OF ENERGY
under contract DE-AC05-00OR22725

CONTENTS

LIST OF FIGURES

ABBREVIATIONS

AM	additive manufacturing
AMMT	Advanced Materials and Manufacturing Technologies
ASME	American Society of Mechanical Engineers
BPVC	Boiler and Pressure Vessel Code
CCD	charged-coupled device
DSCNN	dynamic segmentation convolutional neural network
FBG	fiber Bragg grating
FPC	Fabry–Perot cavity
IR	infrared
LPBF	laser powder bed fusion
OFDR	optical frequency domain reflectometry
SS	stainless steel
TCR	Transformational Challenge Reactor
WDM	wavelength division multiplexer

ABSTRACT

The US Department of Energy's Advanced Materials and Manufacturing Technologies (AMMT) program focuses on accelerating the development, qualification, demonstration, and deployment of advanced materials and manufacturing technologies to enable reliable and economical nuclear energy. Laser powder bed fusion (LPBF) is one of the most popular additive manufacturing (AM) processes for fabricating components with intrinsically complex geometries. LPBF was extensively explored for nuclear applications under the previous Transformational Challenge Reactor program. Additionally, Oak Ridge National Laboratory developed and licensed the Peregrine software and larger digital platform that couples machine learning and in situ data collection during AM to detect anomalies and any evolved defects. The digital platform will be critical to (1) the qualification of AM components for nuclear applications that link location-specific data to macroscopic properties and (2) predict final component performance. Current in situ process monitoring tools are valuable for observing the formation of stochastic flaws, but additional data are needed to predict the resulting microstructures and associated material performance. Rapid cooling rates and large thermal gradients have caused large heterogeneities in the microstructure, which cause anisotropy in mechanical performance. The AMMT program is evaluating the best approaches for addressing these heterogeneities and their effect on component performance using a combination of multiscale modeling, enhanced in situ process monitoring, and high-throughput experimental testing. This report summarizes strategies for mitigating the risks associated with qualifying AM components, including developing new sensing capabilities for in situ process monitoring and characterizing melt pool solidification and residual stresses to inform multiscale modeling efforts.

1. INTRODUCTION

The US nuclear power industry has been slow to adopt new materials since the first commercial nuclear power plants went online in the late 1950s. In the nearly 70 years since then, incremental advances have been made, including minor modifications to early cladding Zr alloys and steels used in pressure vessel steels. However, today's reactors generally use the same 300 series stainless steels (SSs), Inconel alloys, and Zr alloys developed at the beginning of the 20th century, despite significant advances in alloy development, particularly for advanced high-temperature reactor applications [1-3].

One challenge in deploying any new material is collecting the data required to qualify the material according to applicable standards. For example, qualifying new materials to the American Society of Mechanical Engineers (ASME) Boiler and Pressure Vessel Code (BPVC) is time-consuming and requires extensive materials testing that could take longer than 20 years to satisfy all ASME requirements [3, 4]. Section III, Division 5 of the ASME BPVC specifies only six materials that can be used for pressure-retaining components in high-temperature reactors: SS304, SS316, Fe-2.25Cr-1Mo, 9Cr-1Mo, Alloy 800H, and Inconel 617.

Qualifying new alloys using conventional manufacturing processes is already challenging for risk-averse industries, including the nuclear power industry. Conventional materials manufacturing inhibits complexity in reactor component geometries, often limiting overall component performance and operating conditions, such as temperature [5]. Reactor design development is typically limited to a design-manufacture-learn approach. A more agile design approach that uses rapid prototyping to enable learning during the design and manufacture process before final product completion could reduce inherent risk and enable adaptability to changes in technologies and constraints [5, 6]. For example, the Transformational Challenge Reactor (TCR) program sought to leverage recent advances in advanced manufacturing techniques such as additive manufacturing (AM) to develop a reactor with materials that ASME had already approved, such as SS316 [6, 7]. The main goal of the TCR program was to design a reactor with enhanced passive safety controls and site-specific monitoring that could be easily manufactured, factory-assembled, and deployed to urban and remote locations [7, 8]. Complex geometries could be identified, designed, and printed within 1 week and be ready for evaluation and testing [5, 9].

Using a more manufacturing-driven approach enables control over geometry rather than just choice of materials. AM could transform how nuclear reactor components and systems are designed if a qualification pathway could be established. Without this pathway, the industry will be slow to adopt AM, putting the industry at a significant disadvantage compared with other power generation technologies. To this end, the US Department of Energy's Office of Nuclear Energy has launched the Advanced Materials and Manufacturing Technologies (AMMT) program to develop advanced materials and manufacturing technologies, establish a rapid qualification framework, evaluate materials performance in nuclear reactor environments, and demonstrate and deploy these technologies for nuclear energy applications.

AM enables components to be fabricated by successively adding feedstock material (e.g., powder, sheet) through either a single- or multistep fusion process [10]. One of the more common AM technologies that the TCR program used was laser powder bed fusion (LPBF), which involves selectively laser-melting regions of a powder bed layer by layer. However, the complex melting, and solidification process can result in stochastic defect formation and associated uncertainties in the local microstructure, properties, and the ultimate quality of components fabricated via LPBF. These complexities and uncertainties complicate the ability to guarantee properties and performance, which are necessary for qualifying AM components for nuclear applications. The TCR program laid the foundation for qualifying AM-processed reactor components [11-14], but significant work remains. The general approach relies on integrating recent advances in artificial intelligence, computational modeling, in situ process monitoring, and ex situ characterization and mechanical testing methods into AM processes (e.g., LPBF) to attain more holistic

understanding over component in a build [15]. Coupled with a digital twin, all information relevant to a specific component was saved and archived on a digital platform, enabling design and build data to be integrated with macro- and microstructural characterization and any mechanical or materials performance testing results. Ideally, amassing a data library could inform machine learning algorithms to predict the expected performance of a component based on its in situ monitoring analysis [13, 14].

In situ monitoring of LPBF builds has been explored using multiple techniques, such as visible light optical cameras, near-infrared (IR) cameras, photodiode, high-speed charged-coupled device (CCD) cameras, thermocouples, dual-color pyrometry, and other techniques [16, 17]. The most consistent method for build monitoring is performed with simple visible cameras that image the powder bed after each successive layer; these images can then be processed via image analysis techniques. Machine vision algorithms translate sensor data to a common coordinate system while machine learning algorithms are used to sift through each image and translate the build to specific voxels [18-22]. The algorithm can then be trained to differentiate the anomalous regions observed in each voxel from successfully printed regions. Any stochastic behavior in the printing process can then be detected and reported. Anomalies, defects, and flaws can be distinguished and quantified to an extent, but there is no consensus on or confidence level regarding what defects are acceptable and how they affect component performance.

One significant difference between materials fabricated using LPBF and those fabricated using conventional processing is that cooling rates in LPBF are expected to be 10^5–10^7 K/s, which induces fast solidification kinetics and is uncommon in conventional metals processing (e.g., casting and forging) [23-25]. Flaw and defect formation cannot be understood without a detailed understanding of the cooling rates and the associated thermal gradients. Changes in the melt pool can be correlated to changes in photodiode current and IR images. For example, transitioning from conduction mode (i.e., the melt pool width and depth are similar in length) to keyholing (i.e., the laser penetrates deeply through the vaporization of material, often leaving porosity from unescaped gases at the bottom of the melt pool) can be correlated to changes in photodiode and IR images [26, 27]. If the melt pool behavior can be better quantified during in situ monitoring, any stochastic behavior or transitions in melt pool stability could be related to a potential resulting microstructure and associated material performance. Instruments such as high-speed CCD cameras and pyrometers are intentionally designed to measure the temperature profile of the moving laser and the melt pool. However, balancing fast sampling rates, measurement accuracy, and sensor field of view remains difficult.

Current qualification pathways for metallic components processed via AM and LPBF rely on connecting in situ monitoring data to computational models and ex situ performance data. Although there are many examples of in situ monitoring techniques identifying defects and heterogeneities during the component build, uncertainties in defect detection and their effect on component performance still remain and must be resolved as a part of the qualification process. LPBF uncertainty lies in the thermal history of the printed material, necessitating fundamental measurements of parameters such as melt pool temperature and correlating melt pool behavior to the microstructure and mechanical performance. This report details the most influential factors and heterogeneities expected in as-built LPBF material and outlines potential sensing techniques to measure and map the true thermal history of a build. Ideally, these fundamental sensing techniques will provide necessary ground truth data to inform computational models and complement other more established in situ and ex situ techniques to ultimately guarantee the quality of LPBF-processed components.

2. QUANTIFYING UNCERTAINTY IN LPBF

2.1 RELATING RAPID SOLIDFICATION KINETICS TO PART QUALITY

The most influential LPBF processing parameters include the incoming laser power, raster scan speed of the laser, distance between consecutive scans (i.e., hatch spacing), and powder layer thickness. These parameters are often normalized with an energy density term similar to [24]:

$$Energy\ Density = \frac{Laser\ Power}{Scan\ Speed \times Hatch\ Spacing \times Layer\ Thickness}. \quad (1)$$

Generally, an energy density regime exists in which an alloy can be processed near theoretical density, but voids and porosity are often observed with varying energy densities [25]. Process maps are typically produced each time a machine is used to print a new material to detail the defect evolution with varying processing parameters. An example of the defect evolution for LPBF-processed SS316 is shown in Figure 1(a). Irregular pores due to a lack of fusion are observed at low energy density, an optimized energy density exists in which porosity is minimized but not eliminated, and more circular pores are observed at higher energy density because of the formation of keyholes and the melt boiling. In addition to voids/porosity, the grain structure and potential sub-grain structure also evolve with changing energy density.

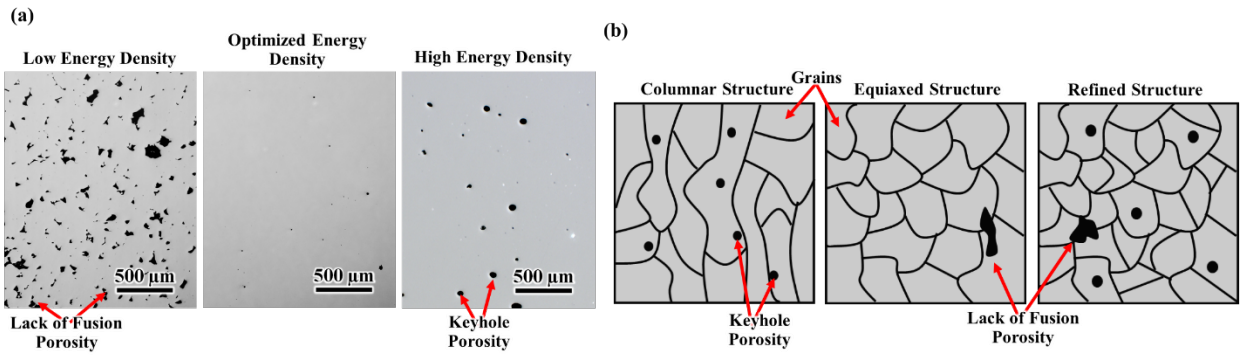

Figure 1. (a) Optical images of SS316L processed with low, optimized, and high energy densities [25, 28]; (b) possible grain structures observed in LPBF-processed components.

Cooling rates in LPBF are between 10^5 and 10^7 K/s, which is faster than conventional solidification processes such as casting (10^1–10^3 K/s) or welding (10^3–10^5 K/s) [23-25]. Higher energy densities typically correspond to higher heat inputs, keeping the material hot for longer and reducing the cooling rate. Contrastingly, lower energy densities typically cool the material quicker and increase the cooling rate because the cooling rate is faster as a result of lower heat input. Microstructural evolution can be understood as a function of cooling rate: the larger the grains, the lower the cooling rate. The rapid cooling rates produce high thermal gradients (10^3–10^4 K/m), forcing a strong dependence of solidification in the direction of the thermal gradient. Moreover, the repetitive melting of each layer can also cause epitaxial grain growth, essentially building the same grain through each consecutive layer, resulting in a columnar (i.e., elongated) structure, as shown in Figure 1(b). Consequently, the directional growth leads to anisotropy in the material properties, including the tensile strength and total elongation. These columnar structures are often observed in the microstructure of materials, even those printed with optimized energy densities for highest part density.

Controlling the laser trajectory and/or cooling rates can limit the directional growth and promote more equiaxed structures, as shown in Figure 1(b). Elimination of directional growth can be accomplished by

varying the laser energy density and the scanning direction of the laser between each layer. Moreover, material composition may promote the growth of more equiaxed or more columnar structures. Ideally, the microstructure could be refined but not without promoting defect formation, as shown in Figure 1(b). For example, limiting grain growth would require low energy densities, but lack of fusion porosity becomes a concern. A parameter combination may exist that reduces anisotropy while minimizing porosity. However, even if such a parameter existed, stochastic defect formation remains a concern, as shown in Figure 1(b).

2.2 CURRENT STATE OF THE ART

The Manufacturing Demonstration Facility at Oak Ridge National Laboratory has patented and licensed a deep learning algorithm called the Dynamic Segmentation Convolutional Neural Network (DSCNN) within the ORNL-developed software, Peregrine, for in situ process monitoring and analysis [11-14, 20-22, 29]. Multi-model sensor data, such as visible light or near infrared camera image, are taken before and after each successive layer. Each image is then registered and correlated to slice files that originate from the CAD software used to draw the component in three dimensions. During the slicing operation, a CAD file is horizontally segmented by the powder layer thickness so that each slice becomes the profile for the laser. These slice files can be leveraged not only by the printer but also by the algorithm to identify the laser scan paths.

Peregrine can discretize the camera images into voxels, which accounts for the resolution of the sensor data (typically 100 × 100 μm), and the *z*-vector is equal to the layer thickness (~50 μm) [11, 14]. Each voxel is analyzed for important and different defects, as demonstrated in Figure **2**(a), and compared with printed material [14]. Six example anomaly classes are soot/slag, recoater streaking, incomplete spreading of the powder by the wiper, debris, swelling, and super elevation across the printed layer. Under the TCR program, multiple builds were performed with different geometries, including simple cubic prisms, cylindrical burst tubes, powder traps, thin walls, and geometry stacks with different angled overhangs, such as the TCR Phase 1 Build 2 shown in Figure **2**(b). Four sets of each geometry were printed using different combinations of processing parameters, including the nominal values that the 3D printer manufacturer provided, the values determined to be best for minimal porosity, the values used to induce lack of fusion defects with low energy density, and the values with higher energy density to induce more keyhole-type porosity.

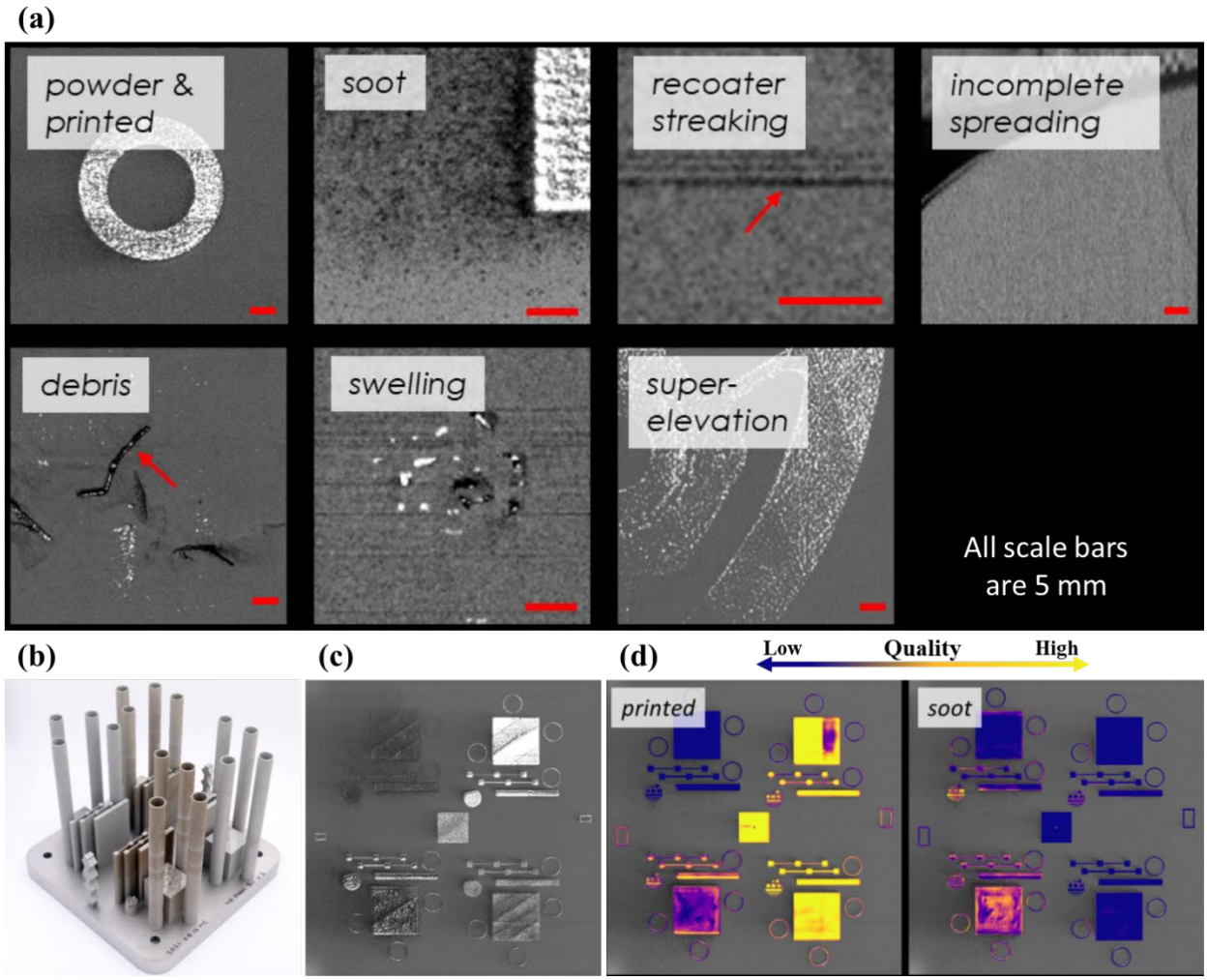

Figure 2. (a) In situ photo of prototypical defects observed during LPBF processing. (b) Photo of the completed TCR Phase 1 Build 2. (c) In situ photo taken during the build [14]. (d) Peregrine analyzes the in situ camera images and determines the percentage of defects vs. successfully printed material. The first image shows the overall quality of the build and total defect formation, but the second image indicates the power of Peregrine to differentiate between defects and map them over the build [14].Figure **2**(c) is a photo taken during the build in which each grouping of parts can be easily distinguished based on differences in the white and black contrast. Figure **2**(d) shows Peregrine's analysis of the printed material and the amount of the soot-type defect present after image-processing one layer. The two clusters of geometries with the most printed material and least soot were the top-right and bottom-right clusters, which were set at the nominal and best parameters. Peregrine visualized the amount of printed material for the two sets of parameters that were most likely to print dense material and compared them with the parameters that produced excessive defects. The inert gas flow moves across the image from right to left. Soot/slag is the material excised during the laser-melting process, and it often oxidizes, making it nonideal to print. Inert gas flow pushes the soot over the bed, enabling the soot particles to deposit over the part. Melting the particles is difficult and may result in inclusions and potential porosity from lack of interparticle fusion.

3. PROPOSED SENSORS AND INSTRUMENTATION

3.1 EXTRINSIC SENSING

All LPBF work will be performed in a Renishaw AM400 unit, shown in Figure 3(a). The Renishaw is equipped with a 400 W pulsed laser, which has a wavelength of 1,070 nm. The total build volume is 250 × 250 × 300 mm, and the minimum build volume is 78 mm^3. Powder is gravity fed from the top of the printer down through a gate that opens in the back of the printer. During a build, powder is dispensed into the build chamber by opening the gate and is then spread over a starting substrate (i.e., build plate) using a wiping mechanism. The laser is focused from the top of the chamber over the center of the build plate.

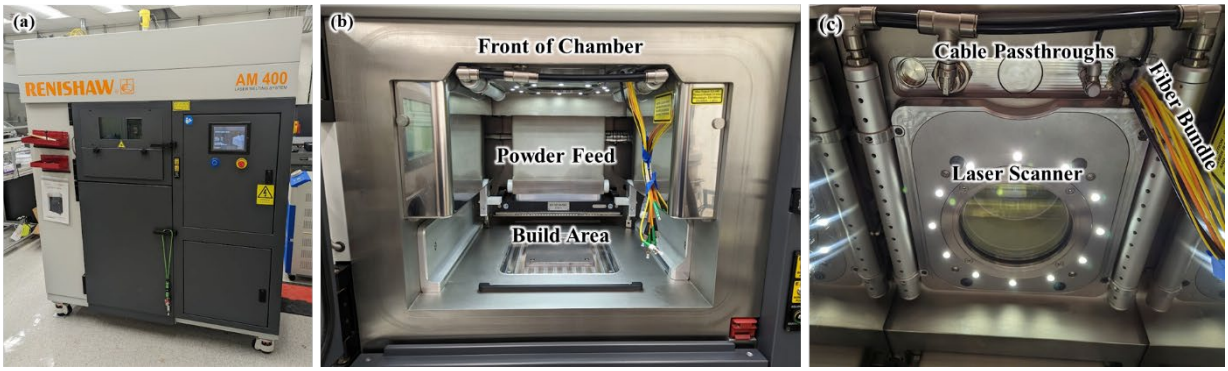

Figure 3. (a) Renishaw AM400 unit, (b) build chamber, and (c) location of the cable passthroughs for any sensors. A bundle of different fiber-optic connectors is shown in the top right of (b) and (c) feeding through one of the passthroughs.

A visible (Basler) and near-IR (Pixelink) camera was mounted in the build chamber, as show in Figure 4. Three passthroughs are located at the top of the build chamber close to the door, as pictured in Figure 3(c). The cameras were housed in protective covers and mounted at specific positions to remain out of the laser scan space. Camera images were then processed with the Peregrine software so that defect data could be analyzed and correlated with any post-build characterization data. Recent studies correlated the defects identified by Peregrine-processed images to those that use x-ray computed tomography data [22, 29].

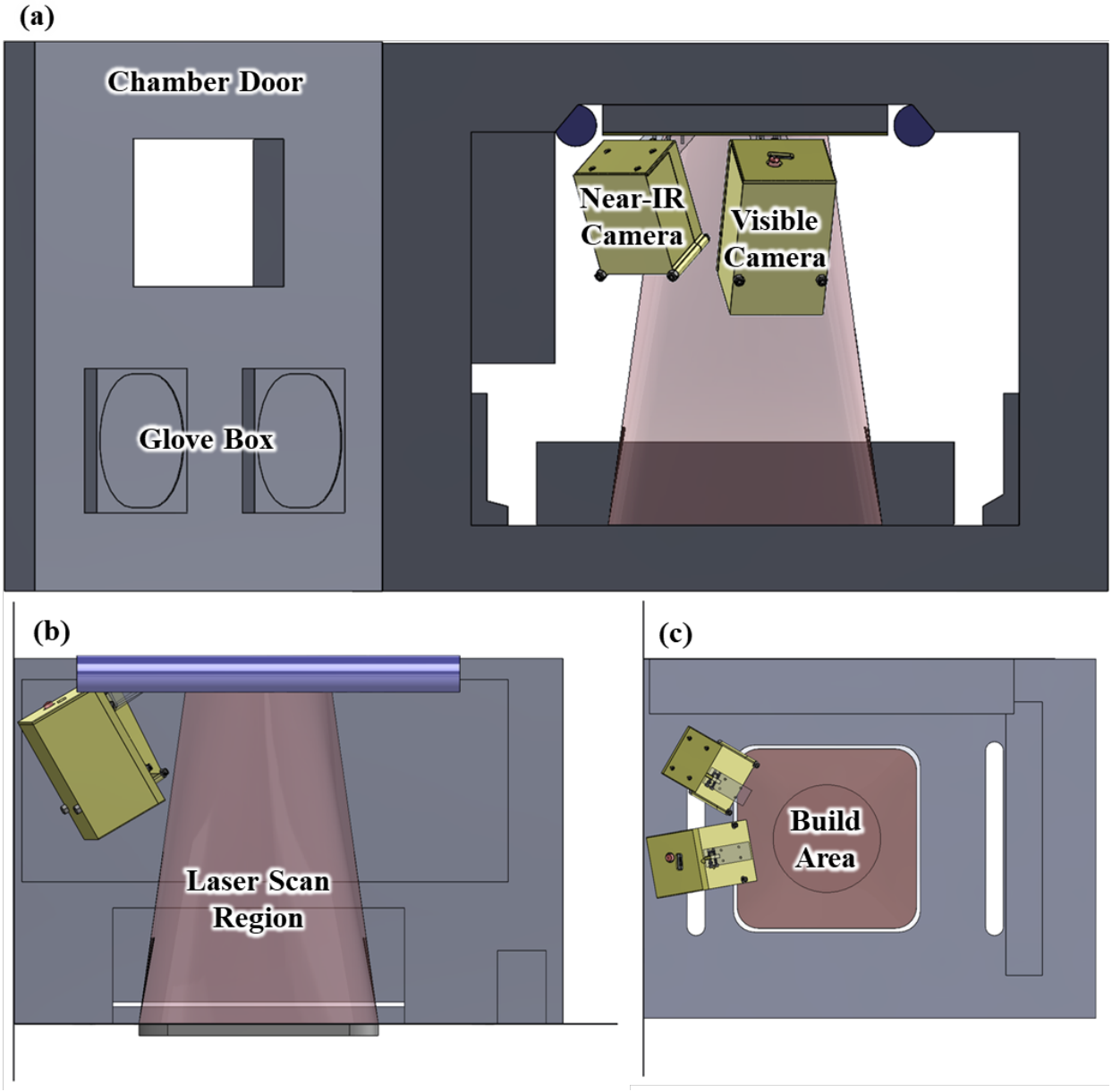

Figure 4. CAD models of the Renishaw AM400 with the installed camera sensors showing the (a) front, (b) side, and (c) top of the build chamber.

3.2 HIGH-SPEED TEMPERATURE MEASUREMENTS

High-speed temperature measurement techniques rely on detecting radiation from a heated surface. Near-IR cameras and other similar measurement devices enable thermal mapping but are limited by their number of pixels and the detector scan frequency [13]. Collection with these devices is generally slow and dependent on the pixel size used. Decreasing the pixel size will greatly increase the processing time, reducing collection rates. Moreover, calibrating the signal intensity read by the camera to a temperature remains difficult because of varying changes in the emissivity of the material that occur during the melting and solidification process [13, 30]. Even if the emissivity could be accounted for, a plume is generated during the laser-melting process in LPBF, obscuring true melt measurement. The plume itself

will have an associated radiation that could interfere with data collection and understanding the true melt pool temperature.

Pyrometers operate similarly to near-IR cameras because both depend on collecting light through an optic that is transmitted to one or more photodetectors [30]. Multiwavelength pyrometers are often used because of their simple design and ease in signal processing, but using two-color pyrometers can be independent of variations in emissivity after initial calibration, making them ideal for accurate temperature sensing [30]. Using small probe diameters, such as integrated fiber optics (<1 mm in diameter), enables the sensor to be easily positioned at an angle below the plume during the laser-melting process so that the true melt temperature can be measured. Additionally, sampling from the pyrometer is rapid since data collection is purely reliant on radiating light detection, not limited by pixel resolution as might be the case with IR cameras. Therefore, pyrometry can be performed at high speeds, which is ideal for capturing the cooling rates associated with LPBF.

The proposed pyrometry setup uses a multimode OM1 fiber optic (62.5 μm core diameter) to collect and transmit light. Fiber optics are commercially available, easy to handle, and resistant to high temperatures (up to ~1,000°C for silica-based fibers). Additional collimators can be added to increase the collection radius of the fiber to 5–20 mm during the laser-melting process, as shown in Figure 5(a). The broadband transmitted spectrum is split using a wavelength division multiplexer (WDM), as shown in Figure 5(a). The WDM uses fiber Bragg gratings (FBGs), which are etched patterns in the fiber intended to reflect specific wavelengths of light. Once light enters the fiber, the FBGs split the collected spectra into two wavelengths: 850 and 1,310 nm. In this way, all other wavelengths are filtered, including the wavelength of the laser in the printer (1,070 nm). InGaAs photodetectors are used to read the intensity of the separated spectrums. The expected intensity (I) from each wavelength (λ) can be expressed as under Wein's approximation [30, 31]:

$$I_\lambda = \frac{C_1 \varepsilon_\lambda}{\lambda^5 e^{\frac{C_2}{\lambda T}}}, \tag{2}$$

where C_1 and C_2 are Planck's radiation constants, ε_λ is the wavelength-dependent emissivity of the measured object, and T is the temperature. Pyrometer calibration involves sampling with the pyrometer during controlled heating of a desired material via thermocouple control. A relationship between the thermocouple temperature and the ratio between the intensities of the photodetectors can be used to accurately measure the melt pool temperature measured by the photodetectors. Preliminary testing will also include needed steps for filtering out the radiating light from the plume of the melt to ensure accurate measurements.

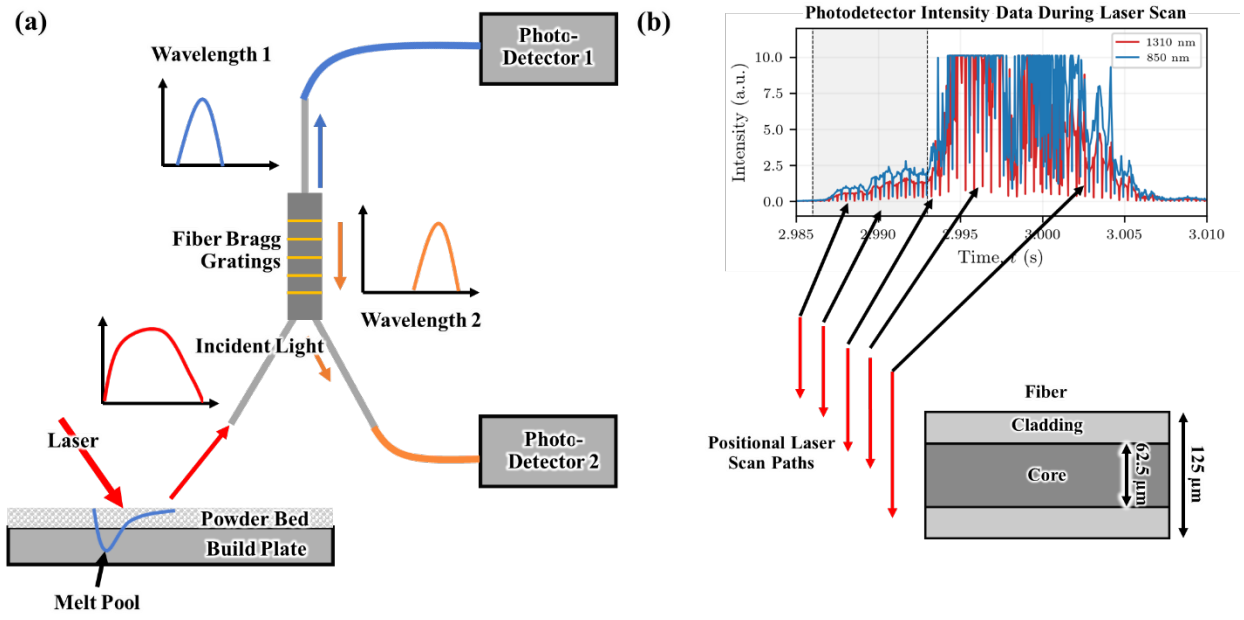

Figure 5. (a) Schematic of the pyrometer setup, including the FBGs used to filter the incident light inside the WDM; (b) sample data taken from the pyrometer during laser scanning. The intensity of the spectrum appears as a bell curve because the laser scans across the build plane at varying distances from the fiber. Light detected near the line of sight of the core is expected to be more intense than light detected at the edges of the fiber.

The initial design of the two-color pyrometer was used to detect the radiation emitted during laser scanning. Data collection was made possible by a data acquisition system sampling at 50 kHz. During testing, the fiber was laid flat on a steel build plate. The laser was positioned ~40 mm from the front of the fiber and scanned perpendicular to the fiber using a laser power of 200 W and a scan speed ~300 mm/s. The recorded spectra that the fiber detected during the laser scanning are shown in Figure 5(b). A quasi-normal curve was observed and can be correlated to the position of the laser with respect to the fiber core. Radiated light is coupled into the fiber within a given acceptance cone defined by the radius of the fiber and the distance between the fiber and melt pool. The intensity fluctuations in Figure 5(b) result from the melt pool moving parallel and perpendicular to the fiber axis, and higher intensities are observed when the melt pool is within the line of sight of the fiber and when the melt pool is closer to the end of the fiber.

The pyrometer has many local minima and maxima separated by ~500 µs. The laser dwell time was expected to be 120 µs, and delay time was expected to be 10 µs. Because these initial data were collected at a relatively low frequency of 50 kHz (approximately every 20 µs), the data acquisition system was unable to detect the delay time of the laser. Moreover, the photodetectors had not been optimized for such high collection rates. However, the pyrometer is sensitive enough to measure changes that the pulsing laser induces. Possible improvements include increasing the sampling rate with additional hardware to ideally collect at approximately megahertz frequencies. This will require advanced triggering to be incorporated into the data collection and online processing to determine peak melt pool temperatures and cooling rates.

3.3 SUBSURFACE DISTRIBUTED SENSING

Although pyrometry supports the fast-sampling rates required to properly quantify the associated cooling rates with LPBF processing, the technique can measure only the maximum melt pool temperature on the surface of the component at locations that the fiber acceptance cone constrains. Additional optics could be inserted to modify the pyrometer so that it observes a wider range of the powder bed, possibly by using the laser scanner to reflect light toward the pyrometer or by adding additional reflectors or collimators in the build chamber [32]. However, modifying commercial printers to enable control over the laser optic system is difficult and could damage printer functionality. Additional reflectors or collimators must be properly placed at low angles to avoid the powder plume, as discussed previously. Therefore, to map temperature profiles near the localized solidification, other instrumentation is required that can inform the calibration of extrinsic sensors, such as near-IR cameras, to record temperature profiles more accurately across the powder bed. Moreover, the ability to place sensors below the build plane could provide valuable data regarding melt pool solidification to inform and calibrate computational models.

Optical frequency domain reflectometry (OFDR) is an optical technique that has been demonstrated for spatially distributed temperature and strain measurements in fiber-optic sensors [33]. As shown in Figure 6(a), an incident spectrum is directed down a fiber optic via a tunable laser source that typically has a wavelength centered at approximately 1,550 nm. The backscattered spectrum results from the weak Rayleigh backscattering of light or from stronger reflections caused by FBGs. The fibers are clad with a material that has a refractive index similar to the silica core, which prevents light from escaping the fiber. The same material used in the cladding is used to terminate the end of the fiber to help bleed what remains of the incident spectrum and to prevent any large back reflections that might obscure the lower intensity Rayleigh backscatter signal.

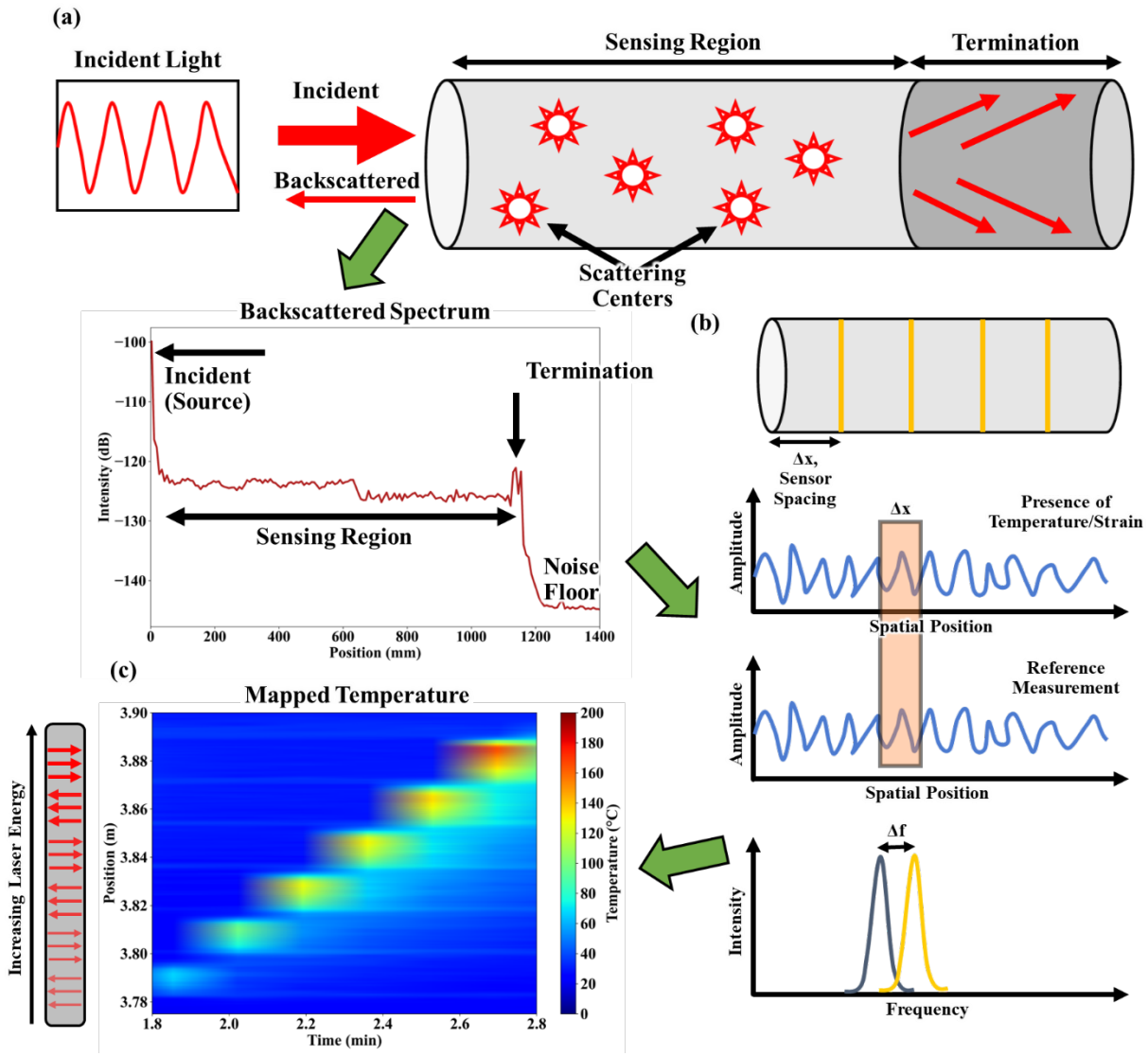

Figure 6. Schematic of (a) the Rayleigh backscattering of light and OFDR, (b) processing the backscattered spectra using Fourier transforms to isolate reflected spectra at specific locations, and (c) an example spatial map of subsurface temperatures along a fiber during in situ temperature testing of an LPBF build processed with varying laser energy.

OFDR scans can be taken during the control state (e.g., at room temperature, under no strain) and during the presence of an applied temperature or strain. The reference scan and subsequent scans can be correlated to determine a spectral shift, as shown in Figure 6(b). Fourier transforms can be used to compare the beat frequencies in the amplitude with frequency data, isolate specific frequencies corresponding to specific locations along the fiber, and transform the isolated data back into the spectral domain to provide intensity spectra originating from one sensor "gauge" location along the fiber. The spectral shift ($\Delta\nu$) between the active and reference scans can then be calibrated to a temperature (T) or strain (ε) [33]:

$$\frac{\Delta\nu}{\nu} = K_T \times \Delta T + K_\varepsilon \times \varepsilon, \tag{3}$$

where ν is the center optical frequency, and K_T and K_ε are constants.

The efficacy of OFDR in LPBF was tested by embedding a SS316L sheath (~800 µm outer diameter and ~356 µm inner diameter) and inserting a polyimide-coated single mode silica fiber optic (250 µm outer coating diameter, 125 µm cladding diameter, and 9 µm core diameter). The fiber was continuously interrogated with an ODiSI-6000 (Luna Innovations) and sampled at 10 Hz, and the gauge length was set to 0.65 mm. To embed the sheath, six 20 mm wide blocks were printed over the top of a 100 mm long section of the sheath using SS316L powder feedstock (Renishaw). The blocks were scanned from left to right, as shown in Figure 6(c), using increasing laser powers of 100, 150, 200, 250, 300, and 350 W. All other parameters were held constant, including powder layer thickness (0.05 mm). Increasing laser power is expected to increase the total input energy, resulting in a larger temperature profile in the base. A segment during the laser exposure is mapped spatially in Figure 6(c) in which six discrete temperature maxima correspond to a width of ~20 mm. Moreover, the temperature magnitude increased as laser energy input increased.

Although OFDR is a powerful tool for distributed sensing, the sampling rates are low and have a maximum scan frequency of <100 Hz. This scanning frequency is limited by the time required to scan the tunable laser and perform the complex Fourier analysis to determine spatially distributed temperatures. The map in Figure 6(c) distinguishes differences in temperature among the different blocks printed. However, the overall magnitudes are lower than the expected temperatures produced during the laser melting process, partially due to the software's inability to detect large, rapid changes in temperature from the relatively weak Rayleigh backscattered signals. Therefore, a more rapid collection method is preferred for distributed sensing that can spatially map temperature and enable faster sampling to help better capture the fast solidification kinetics in LPBF processing.

Fabry–Perot cavities (FPCs) are one option for measuring dynamic changes in temperature or strain at one location[34]. FPCs can be interrogated using a wide range of techniques, some of which allow sampling frequencies on the order of megahertz or higher. FPCs rely on the interference pattern generated by light reflections that occur at the end of the fiber and at a second surface spaced some distance from the end of the fiber. The main drawback of FPCs is that they are point sensors and cannot be used for distributed sensing. Alternatively, FBGs can be inscribed along the length of an optical fiber with varying Bragg wavelengths. When interrogated with a tunable laser source, the peak wavelengths can be monitored without requiring the complex Fourier analysis used to perform distributed sensing based on Rayleigh backscatter. The higher reflectivity of FBGs and their unique spectral features make it easier for software to evaluate larger, rapid changes in the FBG wavelength (i.e., temperature). Figure 7 shows an example of how FBGs could be inscribed along the length of the fiber, as well as a typical interference spectrum from a fiber with multiple FBGs that each have their own unique wavelength. With this approach, spatially distributed measurements can be performed at high frequencies to measure large, rapid changes in local temperatures. The spatial resolution is limited by the range of the tunable laser and potential overlap in the wavelength domain between adjacent gratings.

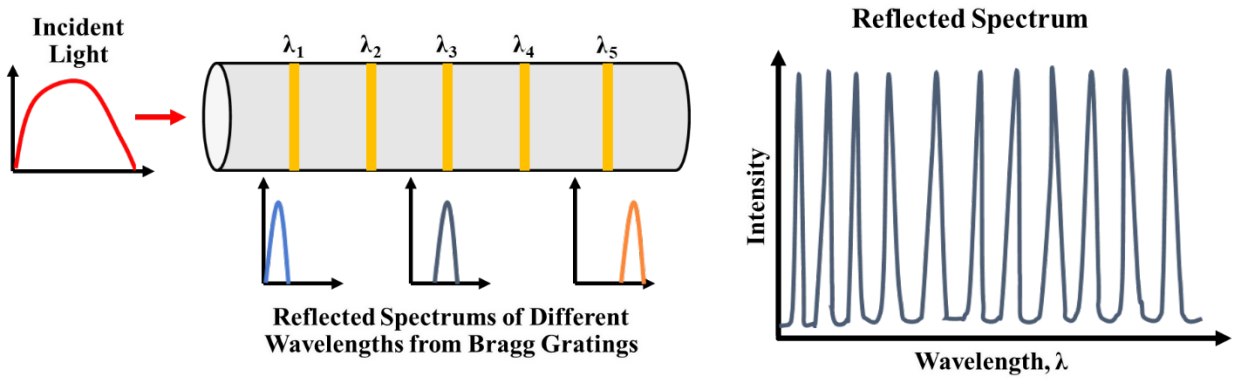

Figure 7. Functionality of an FBG array scanned with swept wavelength interferometry.

The current setup for interrogating FBGs uses a Hyperion (Luna Innovations) system that can collect at 5 kHz. Although slower than the pyrometer, the system is significantly faster than what can be achieved using OFDR and relying on the complex processing of Rayleigh backscattered signals. The overarching goal would be to obtain the peak melt pool temperatures and cooling rates via pyrometer and correlate them to the subsurface measurements recorded with these distributed techniques.

3.4 MAPPING RESIDUAL STRAIN

The fast solidification kinetics during LPBF and associated spatial temperature gradients can also result in high residual stresses. Residual stress in LPBF-built parts causes warpage and distortion of the surface and edges, which affects the desired geometric tolerances. In situ measurements of residual stress help explain how these stresses can vary with changes in cooling rate as a result of changes in geometry, scan path, or laser parameters.

If fiber-optic sensors are mechanically coupled to the desired component, then OFDR can be used to measure strain along the length of the fiber. To embed fibers in metals using LPBF for strain sensing, metal-coated fibers with an optimized diameter (<360 μm) are chosen to allow the laser to penetrate far enough into the sensor coating so that it bonds with the matrix without causing fiber failure. A fiber scan can be measured before and after embedding to calculate an effective residual strain, as shown in Figure 8(a). A relatively constant compressive strain is observed over an ~20 mm length, which was the target embedding length.

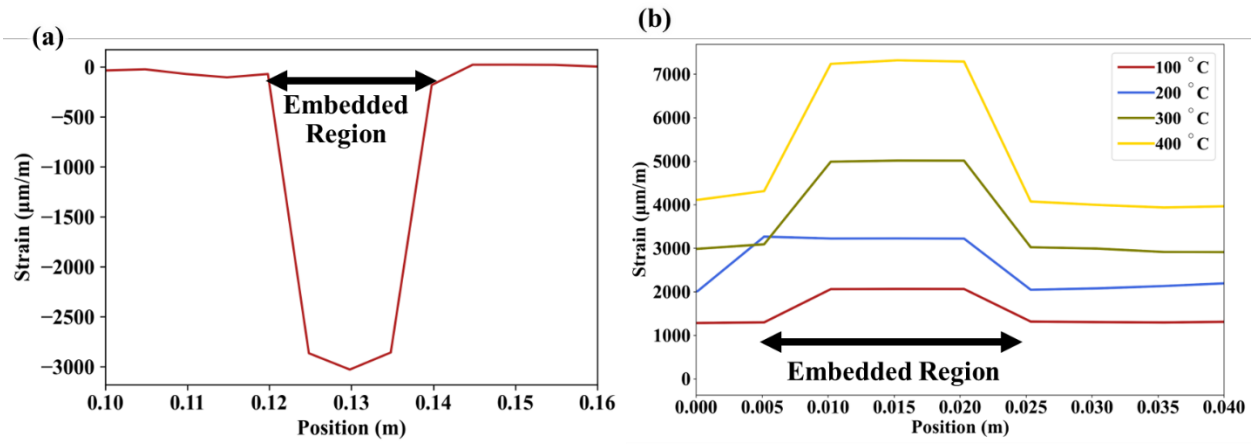

Figure 8. Spatially mapped (a) residual strain imposed on the fiber after embedding and (b) strain evolution for an embedded fiber subjected to increasing temperature.

One challenge of using embedded fiber-optic sensors to measure residual strains is ensuring that the fiber can withstand the thermal strains imposed by the large difference in thermal expansion coefficients between the fiber and the SS316L matrix. An example of continuous strain sensing over the embedded fiber length during high-temperature testing is shown in Figure 8(b). As the temperature increases, the strain read by the fiber increases, but the fiber can withstand bulk component temperatures as high as 400°C.

During LPBF, a combination of the data from Figure 8(a) and Figure 8(b) can be generated. In this combination, the residual stress evolution can be measured after each melted layer by correlating the scan of the fiber before embedding to each subsequent scan taken at the end of each laser scan. Ideally, measured cooling rates from the pyrometer and subsurface measurements can be correlated with the evolved residual stresses. Ground truth data on residual stress can be generated via neutron scattering or high-intensity x-ray diffraction.

Finally, fiber-optic sensors could be used to inform potential changes to LPBF process parameters to correct for increasing residual strain. For example, low transformation temperature metal fillers are commonly used when welding high-strength steels. These materials undergo a martensitic phase transformation and corresponding volumetric expansion upon cooling, which can reduce tensile stresses or even introduce compressive stresses in the heat affected zone. Fiber-optic sensors have been used to quantify compressive residual stresses following weld passes with low transformation temperature filler materials [35]. Similar measurements could be made and LPBF process parameters could be adjusted to reduce local residual stresses in certain regions of components fabricated during AM.

4. SUMMARY

The nuclear industry could greatly benefit from the geometric freedom that AM processes such as LPBF offer. However, the process of qualifying new materials for nuclear applications is complex, time-consuming, and made even more challenging without an established framework for AM processes, inherently resulting in significant heterogeneities in the materials. For example, LPBF cooling rates are expected to be multiple magnitudes higher than those of conventional manufacturing techniques, yielding a high degree of heterogeneity in the microstructure and, subsequently, anisotropy in behavior (e.g., mechanical performance). The general approach to qualifying AM components for nuclear applications seeks to combine in situ process monitoring with computational models and ex situ

characterization and testing. This combination will ultimately detect anomalies and predict the influence of these defects on the resulting microstructure and material performance. However, significant uncertainty still exists in the ability to reliably identify and predict defects, particularly for any stochastically evolved defects. The correlation between the defect formation and microstructure can be measured by understanding the thermal conditions of LPBF material. This paper proposes sensing methods to measure the solidified material cooling rate, resulting thermal history of already solidified material, and evolving residual stresses. In addition to the expected extrinsic sensing techniques already employed using cameras coupled with machine learning algorithms, distributed sensing techniques can leverage single-mode fiber optics to measure temperatures and strains just below the melted surface. Moreover, a fiber-integrated two-color pyrometer will be used to measure the cooling rates. These data seek to reduce the uncertainty in the AM qualification process by informing computational models and improving the data that can be collected in situ during component fabrication.

5. REFERENCES

[1] G.S. Was, D. Petti, S. Ukai, et al., "Materials for Future Nuclear Energy Systems", *J. Nucl. Mater.* 527 (2019) 151837, https://doi.org/10.1016/j.jnucmat.2019.151837
[2] S.J. Zinkle, K.A. Terrani, L.L. Snead, "Motivation for Utilizing New High-Performance Advanced Materials in Nuclear Energy Systems", *Curr. Opin. Solid State Mater. Sci.* 20(6) (2016) 401-410, https://doi.org/10.1016/j.cossms.2016.10.004
[3] S.J. Zinkle, G.S. Was, "Materials Challenges in Nuclear Energy", *Acta Mater.* 61(3) (2013) 735-758, https://doi.org/10.1016/j.actamat.2012.11.004
[4] W. Ren, R. Swindeman, "A Review on Current Status of Alloys 617 and 230 for Gen Iv Nuclear Reactor Internals and Heat Exchangers 1", *Journal of Pressure Vessel Technology* 131(4) (2009), 10.1115/1.3121522
[5] B.R. Betzler, B.J. Ade, A. Wysocki, et al., "Design Downselection for the Transformational Challenge Reactor", Oak Ridge National Lab.(ORNL), Oak Ridge, TN (United States)(2020),
[6] B. Ade, B. Betzler, A. Wysocki, et al., "Transformational Challenge Reactor Design Characteristics", Conference: PHYSOR 2022: International Conference on Physics of Reactors 2022 - Oak Ridge, Tennessee, United States of America - 5/15/2022 8:00:00 AM-5/20/2022 8:00:00 AM, United States, (2022), Medium: ED,
[7] B.R. Betzler, B.J. Ade, P.K. Jain, et al., "Conceptual Design of the Transformational Challenge Reactor", *Nucl. Sci. Eng.* (2022) 1-26, 10.1080/00295639.2021.1996196
[8] N. See, S. Cetiner, B. Betzler, "Design Optimization of the Transformational Challenge Reactor Outlet Plenum", *Nucl. Sci. Eng.* (2022) 1-20,
[9] B.R. Betzler, B.J. Ade, A.J. Wysocki, et al., "Transformational Challenge Reactor Preconceptual Core Design Studies", *Nucl. Eng. Des.* 367 (2020) 110781, ARTN 110781 10.1016/j.nucengdes.2020.110781
[10] W.J. Sames, F. List, S. Pannala, et al., "The Metallurgy and Processing Science of Metal Additive Manufacturing", *Int. Mater. Rev.* 61(5) (2016) 315-360,
[11] A. Huning, R. Fair, A. Coates, et al., "Digital Platform Informed Certification of Components Derived from Advanced Manufacturing Technologies", Oak Ridge National Lab.(ORNL), Oak Ridge, TN (United States)(2021),
[12] L. Scime, J. Haley, W. Halsey, et al., "Development of Monitoring Techniques for Binderjet Additive Manufacturing of Silicon Carbide Structures", United States, (2020), 10.2172/1671401
[13] L. Scime, J. Haley, W. Halsey, et al., "Report on Progress of Correlation of in-Situ and Ex-Situ Data and the Use of Artificial Intelligence to Predict Defects", United States, (2020), 10.2172/1684671
[14] L. Scime, M. Sprayberry, D. Collins, et al., "Diagnostic and Predictive Capabilities of the Tcr Digital Platform", (2021),
[15] C. Hensley, K. Sisco, S. Beauchamp, et al., "Qualification Pathways for Additively Manufactured Components for Nuclear Applications", *J. Nucl. Mater.* 548 (2021) 152846, ARTN 152846

10.1016/j.jnucmat.2021.152846
[16] J.L. McNeil, K. Sisco, C. Frederick, et al., "In-Situ Monitoring for Defect Identification in Nickel Alloy Complex Geometries Fabricated by L-Pbf Additive Manufacturing", *Metall. Mater. Trans. A* 51(12) (2020) 6528-6545, 10.1007/s11661-020-06036-0
[17] J. Raplee, J. Gockel, F. List, et al., "Towards Process Consistency and in-Situ Evaluation of Porosity During Laser Powder Bed Additive Manufacturing", *Sci. Technol. Weld. Joining* 25(8) (2020) 679-689, 10.1080/13621718.2020.1823654
[18] L. Scime, J. Beuth, "Anomaly Detection and Classification in a Laser Powder Bed Additive Manufacturing Process Using a Trained Computer Vision Algorithm", *Addit. Manuf.* 19 (2018) 114-126, https://doi.org/10.1016/j.addma.2017.11.009
[19] L. Scime, B. Fisher, J. Beuth, "Using Coordinate Transforms to Improve the Utility of a Fixed Field of View High Speed Camera for Additive Manufacturing Applications", *Manufacturing Letters* 15 (2018) 104-106, https://doi.org/10.1016/j.mfglet.2018.01.006
[20] L. Scime, D. Siddel, S. Baird, et al., "Layer-Wise Anomaly Detection and Classification for Powder Bed Additive Manufacturing Processes: A Machine-Agnostic Algorithm for Real-Time Pixel-Wise Semantic Segmentation", *Addit. Manuf.* 36 (2020) 101453, https://doi.org/10.1016/j.addma.2020.101453
[21] L. Scime, A. Singh, V. Paquit, "A Scalable Digital Platform for the Use of Digital Twins in Additive Manufacturing", *Manufacturing Letters* 31 (2022) 28-32, https://doi.org/10.1016/j.mfglet.2021.05.007
[22] Z. Snow, L. Scime, A. Ziabari, et al., "Observation of Spatter-Induced Stochastic Lack-of-Fusion in Laser Powder Bed Fusion Using in Situ Process Monitoring", *Addit. Manuf.* 61 (2023) 103298, https://doi.org/10.1016/j.addma.2022.103298
[23] H. Hyer, L. Zhou, A. Mehta, et al., "Composition-Dependent Solidification Cracking of Aluminum-Silicon Alloys During Laser Powder Bed Fusion", *Acta Mater.* 208 (2021) 116698, ARTN 116698 10.1016/j.actamat.2021.116698
[24] H. Hyer, L. Zhou, S. Park, et al., "Understanding the Laser Powder Bed Fusion of Alsi10mg Alloy", *Metallography Microstructure and Analysis* 9(4) (2020) 484-502, 10.1007/s13632-020-00659-w
[25] H.C. Hyer, C.M. Petrie, "Effect of Powder Layer Thickness on the Microstructural Development of Additively Manufactured Ss316", *J. Manuf. Process* 76 (2022) 666-674, 10.1016/j.jmapro.2022.02.047
[26] S.S. Babu, N. Raghavan, J. Raplee, et al., "Additive Manufacturing of Nickel Superalloys: Opportunities for Innovation and Challenges Related to Qualification", *Metall. Mater. Trans. A* 49(9) (2018) 3764-3780, 10.1007/s11661-018-4702-4
[27] J. Raplee, A. Plotkowski, M.M. Kirka, et al., "Thermographic Microstructure Monitoring in Electron Beam Additive Manufacturing", *Scientific Reports* 7(1) (2017) 43554, 10.1038/srep43554
[28] H.C. Hyer, K. Carver, F.A. List Iii, et al., "Embedding Thermocouples in Ss316 with Laser Powder Bed Fusion*", *Smart Mater. Struct.* 32(2) (2023) 02LT01, 10.1088/1361-665X/acae4c
[29] W. Halsey, D. Rose, L. Scime, et al., "Localized Defect Detection from Spatially Mapped, in-Situ Process Data with Machine Learning", *Frontiers in Mechanical Engineering* 7 (2021) 767444,
[30] A. Tapetado, J. Diaz-Alvarez, H. Miguelez, et al., "Fiber-Optic Pyrometer for Very Localized Temperature Measurements in a Turning Process", *IEEE Journal of selected topics in Quantum Electronics* 23(2) (2016) 278-283,
[31] B. Müller, U. Renz, "Development of a Fast Fiber-Optic Two-Color Pyrometer for the Temperature Measurement of Surfaces with Varying Emissivities", *Rev. Sci. Instrum.* 72(8) (2001) 3366-3374,
[32] P.A. Hooper, "Melt Pool Temperature and Cooling Rates in Laser Powder Bed Fusion", *Addit. Manuf.* 22 (2018) 548-559,
[33] K.O. Hill, G. Meltz, "Fiber Bragg Grating Technology Fundamentals and Overview", *J. Lightwave Technol.* 15(8) (1997) 1263-1276, 10.1109/50.618320
[34] D.C. Sweeney, A.M. Schrell, Y. Liu, et al., "Metal-Embedded Fiber Optic Sensor Packaging and Signal Demodulation Scheme Towards High-Frequency Dynamic Measurements in Harsh Environments", *Sensors and Actuators a-Physical* 312 (2020) 112075, ARTN 112075 10.1016/j.sna.2020.112075

[35] C.M. Petrie, N. Sridharan, "In Situ Measurement of Phase Transformations and Residual Stress Evolution During Welding Using Spatially Distributed Fiber-Optic Strain Sensors", *Meas. Sci. Technol.* 31(12) (2020) 125602,